JOURNAL OF CHEMICAL INFORMATION AND MODELING

ARTICLE

pubs.acs.org/jcim

Computational Modeling of the Catalytic Mechanism of Human Placental Alkaline Phosphatase (PLAP)

Gabriela L. Borosky*,† and Susana Lin‡

†Departamento de Matemática y Física, INFIQC, Facultad de Ciencias Químicas, Universidad Nacional de Córdoba, Ciudad Universitaria, Córdoba 5000, Argentina

‡National Health Research Institutes, Division of Environmental Health and Occupational Medicine, No 35, Keyan Road, Zhunan Town, Miaoli County 35053, Taiwan

ABSTRACT: Alkaline phosphatases (APs) catalyze the hydrolysis and transphosphorylation of phosphate monoesters. Quantum mechanical, molecular dynamics, and molecular docking techniques were applied to computationally model the catalytic mechanism of human placental AP (PLAP). Kinetic and thermodynamic evaluations were performed for each reaction step. The functional significances of the more important residues within the active site were analyzed. The role of the metal ion at the metal binding site M3 was also examined. The calculated activation and reaction energy and free energy values obtained suggested the nucleophilic attack of the Ser92 alkoxide on the phosphorus atom of the substrate would be the rate-limiting step of the catalytic hydrolysis of alkyl phosphate monoesters by PLAP. The reactivities of the wild-type M3-Mg enzyme and the M3-Zn protein were compared, and the main difference observed was a change in the coordination number of the M3 metal for the M3-Zn enzyme. This modification in the active site structure lowered the free energy profile for the second chemical step of the catalytic mechanism (hydrolysis of the covalent phosphoserine intermediate). Consequently, a greater stabilization of the phosphoseryl moiety resulted in a small increment in the activation free energy of the phosphoserine hydrolysis reaction. These computational results suggest that the activation of APs by magnesium at the M3 site is caused by the preference of Mg^{2+} for octahedral coordination, which structurally stabilizes the active site into a catalytically most active conformation. The present theoretical results are in good agreement with previously reported experimental studies.

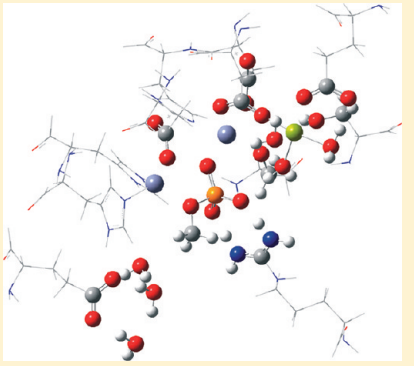

INTRODUCTION

Alkaline phosphatases (EC 3.1.3.1) (APs) form a large family of homodimeric metalloenzymes present in almost all organisms.[1] They catalyze the hydrolysis and transphosphorylation of a wide variety of phosphate monoesters.[2] The enzymatic reaction proceeds through a covalent serine-phosphate intermediate to release inorganic phosphate and an alcohol.[2] Inorganic phosphate is also a strong competitive inhibitor of the enzyme and fills the entire volume of the active-site pocket. In humans, three out of four AP isozymes are tissue-specific, including placental (PLAP), intestinal (IAP), and germ cell (GCAP), while the fourth is a nonspecific thermo sensitive AP (TSAP) found in bone, liver, and kidney.[3]

Alignment of the sequences from a selection of APs from different species shows that the enzyme sequences are very well conserved, especially the active site regions.[4,5] Therefore, the catalytic mechanism, which was deduced from the structure of the *E. coli* AP,[6] was proposed to be similar for eukaryotic APs. Each active site of the dimeric enzyme contains three distinct metal-binding sites (M1, M2, and M3). The M1 and M2 sites are occupied by zinc ions (also referred to as Zn_1 and Zn_2), which play a direct role in the catalytic mechanism.[6] The M3 site is occupied by a magnesium ion which does not appear to be directly involved in catalysis, although it has been shown to be important for full enzyme activity.[7−10] It has also been suggested that a Mg^{2+}-bound hydroxide ion acts as a general base to deprotonate the Ser nucleophile.[6,11] However, recent studies are not consistent with the general base catalysis model and suggest that the Mg^{2+} ion stabilizes the transferred phosphoryl group in the transition state.[12]

Several kinetic and biochemical data have established a two-step reaction mechanism (Scheme 1).[13−15] In the first chemical step, formation of a covalent phosphoserine intermediate E-P (k_2, Scheme 1), Zn_2 is thought to facilitate the generation of a more reactive serine alkoxide, while Zn_1 is considered to stabilize the developing negative charge on the leaving group. In the second chemical step, hydrolysis of the phosphoserine (k_3, Scheme 1), Zn_1 would activate a water molecule for the formation of a hydroxide ion to attack the phosphoryl group, and Zn_2 would stabilize the serine leaving group. In nucleophilic buffers (presence of R_2OH), transphosphorylation to a phosphate acceptor is described by k_5. The rate-determining step of the mechanism is pH dependent; at acidic pH the hydrolysis of the covalent E-P (k_3, Scheme 1) is rate-limiting, while under basic conditions the release of phosphate from the noncovalent enzyme-phosphate

Received: May 23, 2011
Published: September 23, 2011

ACS Publications © 2011 American Chemical Society

Scheme 1

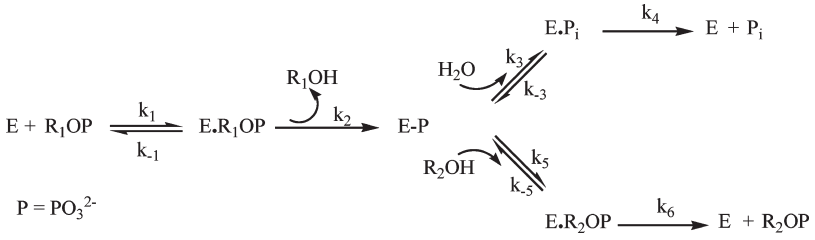

complex ($E.P_i$) (k_4, Scheme 1) becomes the rate-limiting step.[16−18] A pH value of 10.5 has been determined for optimal PLAP activity, although the physiological pH at the placenta surface is around 7.[19] The hydrogen-bonding network in the immediate vicinity of the active site and the electrostatic field created by neighboring amino acid residues assist phosphate stabilization and catalysis.

The X-ray crystal structure of PLAP has been elucidated with 1.8 Å resolution (PDB entry 1EW2).[20] One of the roles of PLAP at the placental surface may include the transfer of maternal IgG to the fetus.[21−23] It was reported that PLAP stimulates DNA synthesis and cell proliferation in fibroblasts in concert with insulin, zinc, and calcium ions.[24] Furthermore, this isozyme promotes the survival of serum-starved mouse embryos and human fetal fibroblasts.[25] Since it enhances growth and survival of fetal cells, this enzyme may be an important modulator of fetal growth. Alterations of PLAP activity were found associated with several disease conditions, as for example, Chagas' disease.[26] PLAP is also one of the first proteins found to be ectopically expressed by cancer cells, leading to the concept that dysregulation of embryonic genes plays a significant role in cancer progression.[27] Many clinical reports have been published concerning PLAP and its use as a tumor marker.[28−31] Therefore, this enzyme is likely to play an interesting role in cancer diagnosis and therapy.

In the present work, we have applied quantum mechanical, molecular dynamics, and molecular docking techniques to the computational modeling of the catalytic mechanism of PLAP, with the purpose of gaining further insight into its function. Kinetic and thermodynamic evaluations were performed for each reaction step. The functional significances of the more important residues within the active site were analyzed. The role of the magnesium ion at the M3 site was also examined in order to get a better understanding of its importance in full enzyme activity.

COMPUTATIONAL METHODS

Molecular Dynamics (MD) Simulations. Simulations were performed starting from the crystal structure of PLAP at 1.8 Å resolution (PDB entry 1EW2).[20] Repairing of missing residues and atoms was done with Swiss-PdbViewer.[32] All crystallographic water molecules were retained, while the NAG cofactor and the inorganic phosphate anion were removed. A phosphate anion optimized at the B3LYP/6-31+G* level was placed at the position of the original phosphate in the crystal structure.[20] The system was immersed in a rhombic dodecahedron box of TIP3P[33] water molecules, with dimensions 777.3 $(Å)^3$. Five Na^+ cations were added to neutralize the system. Thus, the final system contained the enzyme-phosphate complex, 23314 water molecules, and the added cations, leading to a total of 77216 atoms. MD simulations were performed with the GROMACS 4.0.7 software package,[34] using the Amber99SB force field.[35] Parameters for the phosphate anion were generated with AmberTools 1.4,[36,37] and atomic NPA charges of −1.362 *e* and 2.448 *e* were assigned to O and P atoms, which were determined at the B3LYP/6-31+G* level. Simulations were run in the NPT ensemble at 300 K and 1 bar with periodic boundary conditions. Electrostatic interactions were calculated using the particle-mesh Ewald method.[38,39] Cutoff distances for the calculation of Coulomb and van der Waals interactions were 0.9 and 1.1 nm, respectively. Prior to the dynamics simulations, and in order to optimize the position of hydrogens, inorganic ions, and water molecules, an energy minimization was run using the steepest descent integrator for 4000 steps with an initial step size of 0.1 Å (the minimization tolerance was set to 1000 kJ/(mol.nm)). The optimized system was then equilibrated in two steps: (i) a restrained 50 ps simulation with a time step of 1 fs, applying position restraints to the non-hydrogen protein atoms, and (ii) a restrained 50 ps simulation with a time step of 1 fs, applying position restraints to protein backbone atoms. During equilibration the Berendsen barostat[40] and the velocity rescaling thermostat[41] algorithms were applied. Finally, a 30 ns production run was performed at 300 K and 1 bar with a time step of 2 fs using Berendsen barostat and velocity rescaling thermostat algorithms. All bonds were constrained using the LINCS algorithm.[42] Visualization of the dynamics trajectories was performed with the VMD software package.[43]

Docking Procedure. Three-dimensional coordinates of the PLAP structure were obtained from the Protein Data Bank (PDB entry 1EW2).[20] The two zinc ions and two magnesium ions were retained, whereas the heteroatoms, including the cofactor and phosphate, were removed. All crystallographic water molecules were discarded, except for three molecules completing Mg^{2+} coordination (Wat110 (with charge −1 *e*), Wat1, and Wat421). The AutoDock 4.2 program[44] was employed to perform automated molecular docking in order to model the interaction/binding between PLAP and methylphosphate dianion. Hydrogens were added, nonpolar hydrogens were merged to the atom to which they were attached, and partial charges were assigned to PLAP atoms with AutoDockTools. Different docking calculations were done employing Merz−Kollman or Gasteiger partial charges in PLAP atoms. All histidines were defined as neutral, singly protonated on Hε, except zinc-coordinated histidines (His320, His432, His358), which were singly protonated on Hδ. The amino acid side chains of arginine, lysine, aspartate, and glutamate residues were treated as ionized. B3LYP/6-31+G* NPA, RESP, and Gasteiger partial atomic charges were assigned to methylphosphate dianion in different sets of molecular docking calculations. The active site of PLAP (docking area) was defined using the AutoDock module AutoGrid. The grid site was constrained

dx.doi.org/10.1021/ci200228s |*J. Chem. Inf. Model.* 2011, 51, 2538–2548

Table 1. Results for Molecular Docking Calculations

charge type for PLAP	charge type for ligand	number of clusters (population)	$\Delta G_{binding}$ (kcal/mol)
Merz−Kollman	Gasteiger	2 (98, 2)	−10.58
Merz−Kollman	RESP	2 (98, 2)	−10.35
Merz−Kollman	B3LYP/6-31+G* NPA	4 (85, 8, 6, 1)	−10.94
Gasteiger	Gasteiger	1 (100)	−11.89
Gasteiger	B3LYP/6-31+G* NPA	3 (78, 15, 7)	−11.93

to a 23.62 Å cubic space centered on the original phosphate in the crystal structure.[20] The grid box included the entire binding site of PLAP and provided sufficient space for translational and rotational walk of the phosphate ligand. The conformational and orientational spaces of the ligand, and residues Ser92 and Arg166 (defined as flexible) were searched, while the rest of the structure of PLAP was kept rigid. The Lamarckian genetic algorithm (LGA) was applied. Default parameters were used, except that the maximum number of energy evaluations was set to 1.0×10^7. For each of the 100 independent runs performed, a maximum number of 2.7×10^4 genetic algorithm operations were generated on a single population of 150 individuals. Operator weights for crossover, mutation, and elitism were default parameters, 0.80, 0.02, and 1, respectively.

Quantum-Mechanical Calculations. Three-dimensional coordinates of the PLAP structure were obtained from the Protein Data Bank (PDB entry 1EW2).[20] The metal triplet, i.e., both Zn^{2+} ions (M1 and M2) and one Mg^{2+} ion (M3) were selected, along with their ligands: Asp316, His320, His432, His358, Asp357, Asp42, Glu311, Ser155, and the nucleophilic Ser92 as well as the significant residues Arg166 and Glu429 (hydrophilic pocket).[20] Valence at truncated peptide bonds were completed with hydrogen atoms. Six water molecules were included: three to complete Mg^{2+} coordination (one of them as a hydroxide ion) and three in the vicinity of Glu429. The phosphate ion in 1EW2 was also included and used as a template to build the monoester substrate methylphosphate anion (charge $-2\,e$). The amino acid side chains of arginine, aspartate, and glutamate residues were treated as ionized. Histidines were assigned as neutral, singly protonated on Hδ. In this way, the sum of seven positive charges (two Zn^{2+} cations, one Mg^{2+}, and one arginine) plus eight negative charges (three aspartates, two glutamates, one hydroxide anion, and the methylphosphate dianion) resulted in a net charge of $-1\,e$ for the entire model system.

Calculations were performed with the Gaussian 03 package of programs.[45] Preliminary semiempirical PM3MM[46] minimizations were carried out, and these results were used as starting structures for two-layer QM/QM-ONIOM calculations.[47] Density Functional Theory (DFT) optimizations with the B3LYP functional[48−50] were done for the high layer, which consisted of the three metal cations, the methylphosphate dianion, five water molecules, one hydroxide ion, the carboxylate groups of glutamates and aspartates, and the $-CH_2OH$ groups of serines (37 heavy atoms and 24 hydrogens). The 6-31+G* basis was utilized for C, O, N, P, Mg, and H atoms, while the pseudopotential Lanl2DZ was used for Zn. For the rest of the system (low layer, 73 heavy atoms and 78 hydrogens) the PM3MM method was employed. The active site structure was retained by fixing the coordinates of the backbone atoms (involved in peptide bonds), while coordinates of the other atoms were fully optimized. Harmonic vibrational frequency calculations were performed in order to characterize minima and transition states on the potential energy surface and to provide zero-point vibrational energies, thermal corrections, enthalpies, entropies, and free energies. The electrostatic influence of the environment was taken into account by performing polarized continuum model (PCM)[51−54] computations. A dielectric constant $\varepsilon = 4.0$ was used to model the rest of the protein surrounding the active site. Energy calculations and optimizations at the B3LYP-PCM level were carried out for a reduced system built from the gas-phase optimized structures. In this reduced system, aspartates and glutamates were replaced by acetate ions, serines were represented by ethanol, arginine was replaced by acetamidine, and histidines were modeled by 5-methylimidazole (63 heavy atoms and 66 hydrogens).

RESULTS AND DISCUSSION

Molecular Dynamics Simulations. MD calculations for the native protein in aqueous solution provided a stable trajectory for the 30 ns simulation time, as could be seen by inspecting the fluctuations in both the potential energy and the positional root-mean-square deviation (rmsd, computed using the initial crystal structure as the reference structure (PDB entry 1EW2)[20]) determined for the heavy atoms in the protein along the simulation. A large fraction of the structural flexibility derived from the N-terminal region (residues 1−25), whose rmsd was around 16.3 Å. In contrast, the main fold of the protein core (residues 26−479), which comprises the active site, was well preserved and exhibited smaller rmsd values (around 2.3 Å). In this way, MD simulations ensured the stability of the crystal structure 1EW2,[20] whose coordinates were used to build the starting structure of the PLAP active site for the quantum-mechanical computations.

Molecular Docking. Calculations employing several sets of charge types for the protein and ligand were performed. However, in all conditions the preferred docking conformations resulted very similar as well as the corresponding binding affinities. Results are summarized in Table 1. In each case, all 100 docking poses of methylphosphate dianion with PLAP generated between one and four clusters. These studies indicated that methylphosphate dianion docks favorably into the active site of PLAP, with $\Delta G_{binding}$ values in a range between −10.35 and −11.93 kcal/mol. In each case, the binding affinity corresponded to the lowest energy pose of the best docked cluster. Similarly to the binding conformation of phosphate in the PLAP crystal structure, the phosphate group of the ligand formed hydrogen bonds with the guanidinium group of Arg166. Moreover, coordination was observed with Zn_1 and Zn_2. Figure 1 illustrates the conformation where the strongest hydrogen bonds were observed, corresponding to the calculation with Merz−Kollman partial charges in PLAP and Gasteiger charges in methylphosphate dianion. This was the lowest energy docked conformation of the most populated cluster, presenting 98 poses clustered within 2 Å rmsd. The main contribution to the interaction energy was electrostatic (−12.61 kcal/mol), while contributions from

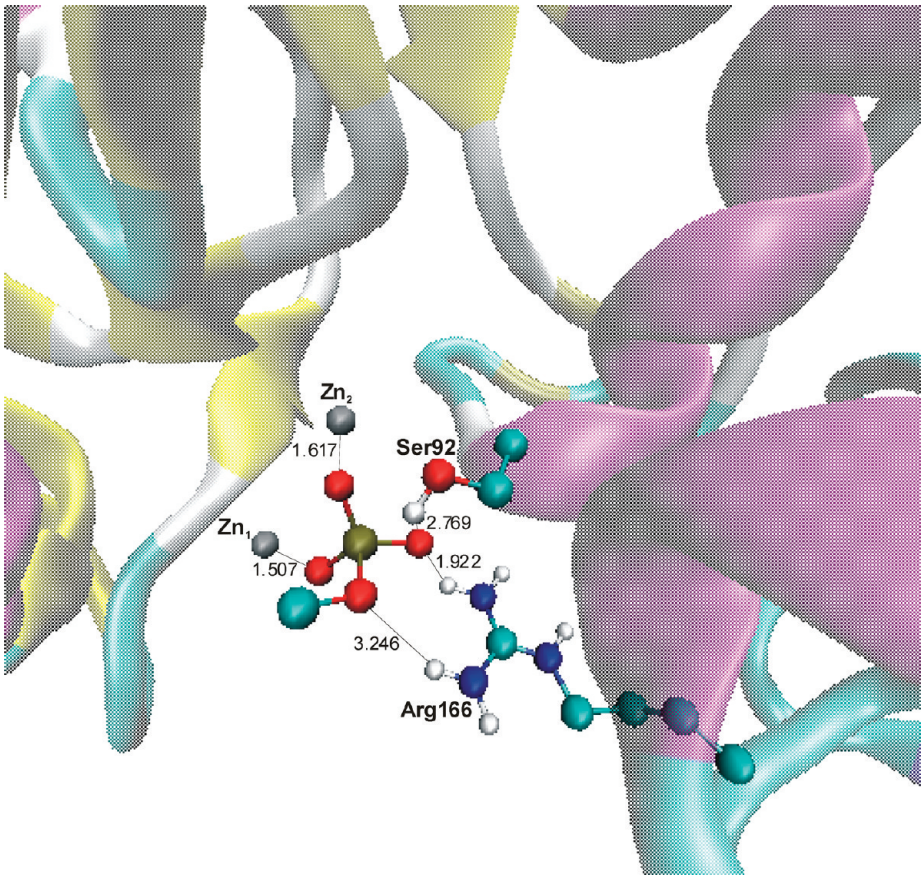

Figure 1. Schematic representation of docking of methylphosphate dianion with PLAP crystal structure.

van der Waals interactions, hydrogen bonding, and desolvation energy summed up to 1.72 kcal/mol.

Quantum-Chemical Calculations. *General Considerations.* The calculation procedure applied was related to the methodology known as cluster approach, that has been successfully employed to model enzymatic reactions.[55,56] In the cluster method, a limited but well-chosen part of the enzyme is cut out to represent the active site and treated quantum mechanically, generally by applying the B3LYP functional. The rest of the protein that it is not explicitly included surrounding the active site may affect the model in two ways. First, by imposing steric constraints on the various parts of the model. If not taken into account, this might lead to large artificial movements of the residues included in the model, as the geometry would adjust to compensate for the lack of surrounding residues, which may result in an incorrect description of the calculated reactions. To model the steric effects, certain key coordinates at the periphery of the model are held fixed from available X-ray structures, typically where truncation is made. Moreover, when low-resolution X-ray structures providing accurate positions of the backbone atoms are available, these atomic positions are fixed during further optimizations of the rest of the structure. Second, polarization provided by the surrounding can affect the computed energies. To model the electrostatic effects, polarizable continuum techniques are usually applied, and solvation energies are used to be obtained from single-point calculations performed on the optimized geometries. A dielectric constant $\varepsilon = 4$ is generally considered to be a good representation of the protein surrounding.[55,56] Systematic studies have shown that as the model size grows, relative solvation effects decrease very quickly because more groups that provide polarization are explicitly included in the model. It has been established that the combination of the coordinate-locking procedure and continuum solvation fruitfully accounts for the parts of the enzyme not included in the model and affords sufficiently accurate calculated energies.[55,56]

In the present work, QM/QM-ONIOM computations were performed for a model consisting of 212 quantum atoms. This model size is considered to yield accurate results by the cluster approach.[55,56] A low-resolution X-ray starting structure (1.8 Å, PDB entry 1EW2)[20] was used, and MD simulations reported above ensured the stability of the crystal structure, particularly the active site region. Test calculations without constraints for the positions of the backbone atoms were carried out as well as computations fixing only some atoms at the periphery of the model (where truncation of the protein was made). However, these test computations evidenced a significant deformation of the active site, probably as a consequence of the lack of steric constraints that the excluded adjacent residues would have imposed. The distorted configurations were probably not compatible with the secondary and tertiary structure of the full protein, and the corresponding changes in energy for reaction steps of the catalytic mechanism resulted in unrealistic values. Moreover, some of the calculations without constraints for the positions of the backbone atoms failed to converge even after more than 800 optimization cycles. By taking all of the above factors into account, it was considered a valid approximation to keep fixed the coordinates of the backbone atoms during all geometry optimizations reported in this study.

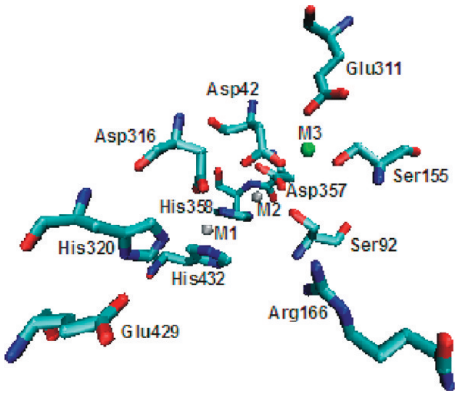

Figure 2. Active site of PLAP and surrounding relevant adjacent residues.

Geometry relaxation of active site residues is certainly important, as recently stated by Sekharan et al.[57] In the present work the side chains of every residue were relaxed. However, reference 57 is a QM/MM study in which the full enzyme has been explicitly included. Because of that, no constraints were necessary to prevent a deformation of the active site upon geometry optimization, as there was no lack of surrounding residues. Instead of applying a QM/MM procedure and including the full enzyme using molecular mechanic force fields, a higher level quantum-chemical method (PM3MM) was employed in the present work for describing the surrounding of the reacting DFT region.

In comparisons between QM/MM (B3LYP/Amber) and QM-only (B3LYP) calculations, it has been indicated that the description of long-range polarization could be one problem in QM/MM calculations.[56] This was mainly ascribed to an overestimation of polarization effects of the QM region by the MM region due to the particular treatment of the electrostatic interactions and the use of a standard (nonpolarizable) force field.[56] This problem was avoided in the present study because the complete system was treated at the quantum-mechanical level.

Wild-Type Enzyme Model. The active site of PLAP involves the catalytic Ser92, the metal triplet (two Zn^{2+} and one Mg^{2+}), Arg166, Glu429, and other amino acids in the immediate vicinity (Figure 2). The hydrophilic pocket formed by Arg166 and Glu429 is considered to stabilize the hydrophilic moiety of the phosphate monoester substrate. Located at the entrance of the cleft that leads to the active site, Glu429 stabilizes the water molecules that bridge the gap to the phosphate moiety of the phosphoserine.[58] As one of these water molecules is highly conserved and involved in the nucleophilic attack on the phosphoseryl intermediate, Glu429 plays a crucial role in this hydrolysis step. In addition, several water molecules are located within the active site and form an extensive hydrogen-bonding network.

The initial structure for the Michaelis complex was built from the molecular docking calculation results. The binding pose presenting the strongest electrostatic and hydrogen bonding interactions within the active site (shown in Figure 1) was selected. The methylphosphate ligand was rotated in order to favor the nucleophilic attack from the catalytic amino acid Ser92. In this way, the oxygen atom from the ester leaving group was coordinated to Zn_1, while two nonbridging oxygens were hydrogen-bonded with the guanidinium group of Arg166.

Geometry optimization of the system constituted by the substrate methylphosphate dianion within the active site of PLAP showed that, in the Michaelis noncovalent complex (Figure 3a), Zn_1 was tetracoordinated by the imidazole nitrogen atoms of His320 and His432, one carboxyl oxygen of Asp316, and one phosphate oxygen atom, with an average metal−ligand distance of 2.07 Å. Zn_2 was pentacoordinated by one of the carboxyl oxygens of Asp357 and Asp42, the hydroxyl of Ser92, the imidazole nitrogen atom of His358, and another phosphate oxygen atom, with an average metal−ligand distance of 2.14 Å. Mg was octahedrally hexacoordinated by the second carboxyl oxygen of Asp42, one carboxyl oxygen atom of Glu311, the hydroxyl of Ser155, and three water molecules, forming a distorted tetragonal bipyramid. The average Mg−O distance was 2.12 Å. While one of these three water molecules was initially included as a hydroxide ion, a proton transfer from the hydroxyl of Ser92 took place leaving the catalytic serine into its ionized form, as it has been suggested.[6,7,59] The two other oxygens of methylphosphate dianion were hydrogen-bonded to the nitrogen atoms of the guanidinium group of Arg166.

The catalytic mechanism of PLAP, illustrated in Scheme 2, was subsequently modeled within the active site. Starting from the noncovalent complex, formation of the covalent phosphoserine intermediate was evaluated (Step 1). The leaving methoxide anion was found to be stabilized by coordination to Zn_1. In Step 2 the methoxide was displaced from metal coordination by a water molecule. The succeeding proton transfer in Step 3 generated methanol and a Zn_1-coordinated hydroxide ion. This hydroxide attacked the phosphoserine (Step 4) to release a hydrogen phosphate anion, restoring the nucleophilic serine oxyanion. The model structures for selected mechanistic steps are displayed in Figure 3, and energy values are shown in Table 2.

The transition state for the first chemical step, i.e., formation of the covalent phosphoseryl intermediate (Step 1, Scheme 2), presented a trigonal bipyramidal structure, consistent with an in-line displacement step, as postulated before by Holtz et al.[60] (Figure 3b). The bond length between the phosphorus atom and the nucleophilic oxygen of serine was 1.933 Å, while the distance from phosphorus to the oxygen atom of the methoxide leaving group was 2.336 Å. Bond forming/breaking oxygens were in opposite axial positions separated by an angle of almost 170 degrees. The three nonbridging oxygen atoms of the transferred phosphoryl group, spaced approximately 120 degrees apart, bisected the axial plane and formed stabilizing interactions with Arg166 and the zinc ions. Zn_1 coordinated the methoxide leaving group, assisting its departure. In the conversion of the noncovalent complex to the covalent intermediate, the side chain of Ser92 underwent a small rotation, and only minor changes were observed in the positions of the other residues, suggesting that the active site arrangement of PLAP is optimal for stabilization of this transition structure.

The second chemical step, involving phosphoserine attack by a nucleophilic hydroxide anion coordinated to Zn_1 (Step 4, Scheme 2), was also an in-line displacement with a trigonal bipyramidal transition state (Figure 3d). The bond length between the phosphorus atom and the oxygen of the leaving serine was 1.898 Å, and the distance from phosphorus to the oxygen atom of the hydroxide nucleophile was 2.513 Å. Stabilizing interactions for this transition structure were very similar to those observed in the first transition state. During this hydrolysis step, only minimal modifications were found in the atomic positions of the included residues, indicating that the active site organization markedly facilitates the catalytic mechanism.

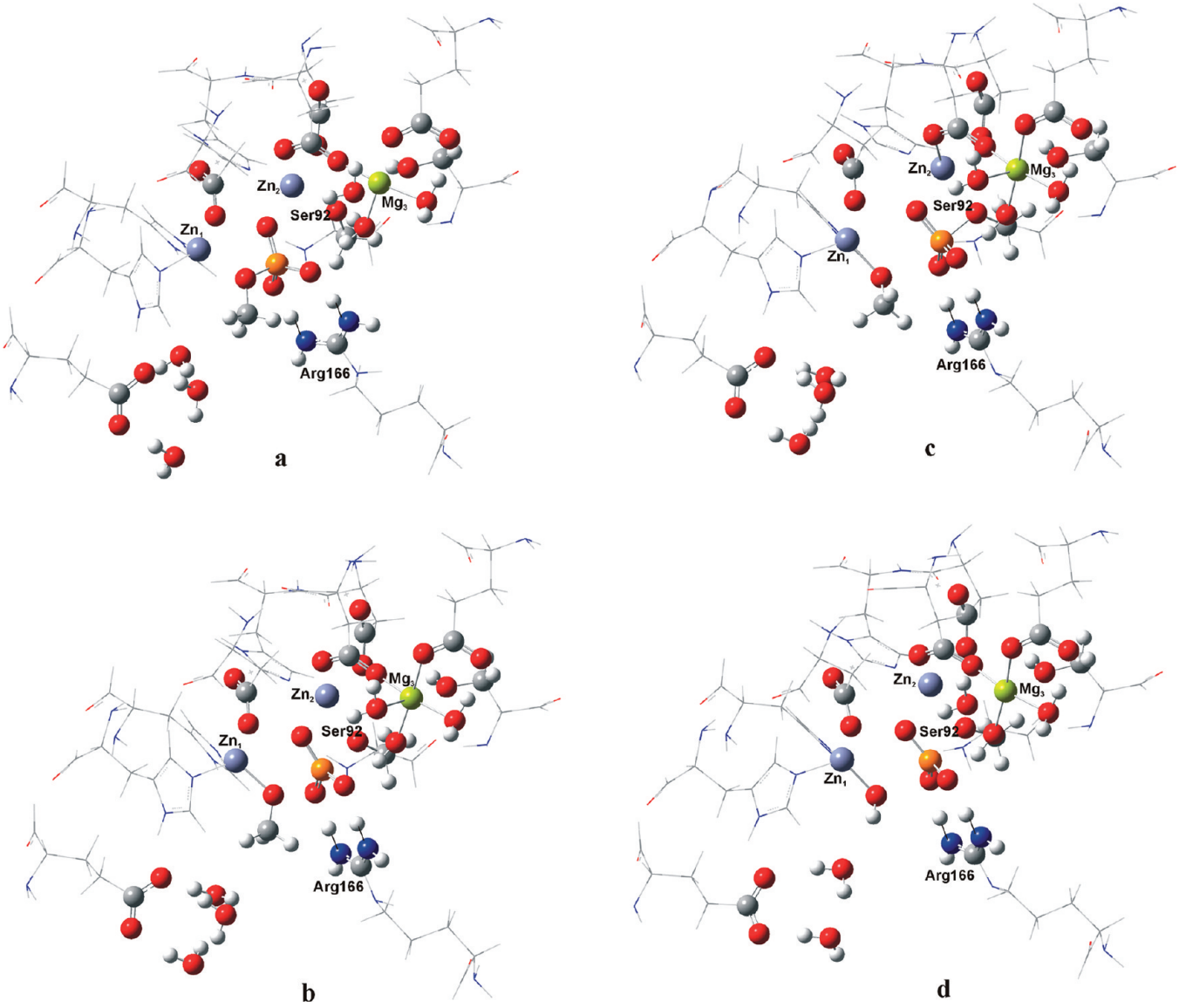

Figure 3. Selected stationary points for the catalytic mechanism. (a) Noncovalent complex. (b) Transition state for serine nucleophilic attack. (c) Phosphoserine intermediate, methoxide anion complexed to Zn_1. (d) Transition state for phosphoserine hydrolysis (methanol left).

Considering the results in Table 2, transition-state theory[61] was applied to estimate the rate constants for the chemical steps 1 ($k_2 = 4.6 \times 10^{-4}$ s^{-1}; $\Delta G^{\neq} = 22.0$ kcal/mol) and 4 ($k_3 = 2.7 \times 10^{11}$ s^{-1}; $\Delta G^{\neq} = 1.8$ kcal/mol) (rate constants nomenclature correspond to the general mechanism illustrated in Scheme 1). These values pointed out the nucleophilic attack of the serine alkoxide to the phosphorus atom as the rate-limiting step for the catalytic mechanism of hydrolysis of phosphate monoesters by PLAP. While for aryl phosphates the rate-limiting step at pH > 7.5 is the product release (k_4), and the hydrolysis of the covalent intermediate (k_3) at pH < 7.5,[16−18] the chemical step of phosphorylation of the enzyme (k_2) has been proposed as rate-determining for alkyl phosphates,[59] in accordance with the present computational results. Considering the experimental rate constant for the noncatalyzed hydrolysis of methylphosphate dianion in water at 25 °C ($k_{exp} = 2 \times 10^{-20}$ s^{-1}),[62] our calculations indicate that PLAP accelerates the reaction by a factor of 2.3×10^{16}. This observation matches the catalytic proficiencies assessed for APs.[63] Thus, the present theoretical results nicely reproduce experimentally determined mechanistic features.

In order to account for the electrostatic influence of the environment, PCM computations were performed employing a dielectric constant $\varepsilon = 4.0$ to simulate the rest of the protein surrounding the active site. Energy calculations and geometry optimizations at the B3LYP-PCM level were carried out for a reduced system built from the gas-phase optimized structures. In this reduced system, aspartates and glutamates were replaced by acetate ions, serines were represented by ethanol, arginine was replaced by acetamidine, and histidines were modeled by 5-methylimidazole. Results are shown in Table 2.

Optimized B3LYP-PCM geometries displayed only small modifications from the gas-phase structures. The displacement from coordination to Zn_1 of the methoxide anion by a water molecule (Step 2, Scheme 2) generated a configuration with two hydrogen-bonding interactions between the oxygen atom of the

Scheme 2

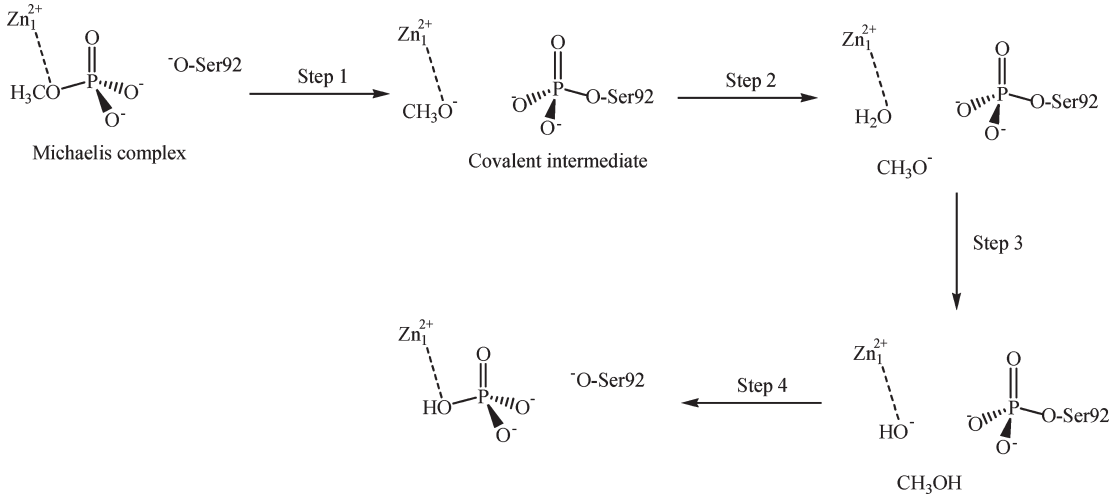

Table 2. Changes in Reaction and Activation Energies and Free Energies Calculated for the Hydrolysis of Methylphosphate Dianion by PLAP[b]

		change in energy [free energy] (kcal/mol)					
		step 1		step 2	step 3	step 4	
protein	method	ΔE_r [ΔG_r]	$\Delta E^{\neq}$ [$\Delta G^{\neq}$]	ΔE_r [ΔG_r]	ΔE_r [ΔG_r]	ΔE_r [ΔG_r]	$\Delta E^{\neq}$ [$\Delta G^{\neq}$]
wild-type enzyme (M3-Mg)	gas phase	16.4 [18.3]	19.6 [22.0]	−10.9 [-11.7]	2.5 [4.3]	−23.2 [-27.0]	3.1 [1.8]
	PCM (single-point)[a]	12.2	8.6	9.4	−17.1	−10.9	0.5
	PCM (optimization)[a]	16.7	17.1	7.6	−17.5	−12.0	6.7
M3-Zn	gas phase	16.1 [18.1]	18.6 [21.0]	−24.6 [-21.4]	4.8 [5.5]	−8.1 [-10.3]	3.8 [5.5]

[a] B3LYP-PCM calculations on a reduced model system (see text and Computational Methods section). [b] Reaction steps are illustrated in Scheme 2.

leaving group, the mentioned water molecule, and a hydrogen atom in His432. While in the gas phase (ε = 1.0) this arrangement was more stable than the methoxide anion coordinated to zinc, in a more polar environment (ε = 4.0) the electrostatic interaction methoxide-Zn^{2+} was preferred. Another important difference was observed for the proton transfer from the Zn_1-coordinated water molecule to methoxide anion to yield hydroxide anion and methanol (Step 3). This reaction was slightly endothermic in gas phase but fairly exothermic according to the PCM calculations. Furthermore, the hydrolysis of the phosphoserine with release of hydrogen phosphate anion (Step 4) was more exothermic in gas phase than in the model with a more polarized protein environment (ε = 4.0).

M3-Zn Enzyme Model. The optimized Michaelis complex was very similar to the structure found with Mg at M3 (Mg_3, wild-type enzyme). Zn_3 was octahedrally hexacoordinated by the same atoms that Mg^{2+} in the wild-type enzyme, also forming a distorted tetragonal bipyramid. The average Zn−O distance was 2.16 Å, slightly larger than for Mg. Similarly, proton transfer from the hydroxyl of Ser92 to the hydroxide anion lead to the ionized form of the catalytic serine. Moreover, the resulting covalent phosphoserine intermediate was comparable in structure to the wild-type model. These observations were reflected in the energetic of this first chemical step of the catalytic mechanism, which presented equivalent values for the changes in free energies of reaction and activation for both active sites with different M3 metals (Table 2).

Displacement of methoxide ion from Zn_1 coordination by a water molecule (Step 2, Scheme 2) modified the configuration of the M3 site, and as a result Ser155 and Glu311 were no longer coordinated to Zn_3. Instead, one of the phosphate oxygen atoms was coordinated to Zn_3, which presented pentacoordination in the form of a distorted square pyramid. This reorganization of the active site generated a stronger phosphoserine bond (1.699 Å vs 1.757 Å in the wild-type enzyme) and slightly decreased the distance between the phosphorus atom and the nucleophilic Zn_1-coordinated water molecule (3.423 Å vs 3.474 Å in the wild-type model). These structural changes originated a more exothermic displacement of the methoxide anion from Zn_1-coordination for the M3-Zn protein (Table 2). Zn_3 pentacoordination was conserved in the subsequent steps. Consequently, the proton transfer from the Zn_1-coordinated water molecule to methoxide anion to give hydroxide anion and methanol (Step 3) was moderately more endothermic than for the wild-type enzyme. Besides, the hydrolysis of the phosphoserine (Step 4) was markedly less exothermic for the M3-Zn enzyme, and the activation free energy for this second chemical step became slightly higher (Table 2). The respective stationary points with Zn_3 octahedral coordination were also characterized. However, the minima for the octahedrally coordinated Zn_3 structure with a water molecule coordinated to Zn_1 could not be isolated as a minimum. Instead, a configuration presenting a small imaginary frequency ($-45\ cm^{-1}$) was considered for the energetic analysis in Table 3.

dx.doi.org/10.1021/ci200228s |J. Chem. Inf. Model. 2011, 51, 2538–2548

Table 3. Changes in Reaction and Activation Energies and Free Energies Calculated for the Hydrolysis of Methylphosphate Dianion by M3-Zn PLAP in Gas Phase[a]

	change in energy [free energy] (kcal/mol)					
	step 1		step 2	step 3	step 4	
Zn_3 coordination number	ΔE_r [ΔG_r]	$\Delta E^{\neq}$ [$\Delta G^{\neq}$]	ΔE_r [ΔG_r]	ΔE_r [ΔG_r]	ΔE_r [ΔG_r]	$\Delta E^{\neq}$ [$\Delta G^{\neq}$]
6	16.1 [18.1]	18.6 [21.0]	−12.5 [-11.8]	4.0 [4.8]	−19.6 [-21.9]	5.7 [7.2]
5			−24.6 [-21.4]	4.8 [5.5]	−8.1 [-10.3]	3.8 [5.5]

[a] Reaction steps are illustrated in Scheme 2.

In the transition state for Step 4 with pentacoordinated Zn_3, the P−O(Ser92) distance was 1.938 Å, and the P−O(hydroxide) bond length was 2.111 Å. On the other hand, for the transition state with octahedral hexacoordination for Zn_3, which resulted in 13 kcal/mol higher in free energy, these bond distances were 1.898 Å and 2.513 Å, respectively. Thus, the most stable square pyramidal structure represents a late transition state, in accordance with the minor exothermicity of the reaction path with pentacoordinated Zn_3. In this way, the most favored Zn_3 pentacoordination lowered the energy profile for the second chemical step. Both transition states are displayed in Figure 4, and the corresponding free energy profiles are shown in Figure 5.

Role of the M3 Metal Ion: Comparison of the M3-Mg vs the M3-Zn Enzymatic Pathways. The main difference between the wild-type M3-Mg enzyme and the M3-Zn protein was the change in coordination number of Zn_3 upon displacement of methoxide anion from Zn_1-coordination by a water molecule. This modification in the active site structure, related to the preference of Zn cations for tetrahedral over octahedral coordination,[64] brought about a lowering of the free energy profile for the second chemical step of the catalytic mechanism (Figure 5), i.e., hydrolysis of the covalent phosphoserine intermediate. However, the greater stabilization of the phosphoseryl moiety, caused by complexation of one of the phosphate oxygen atoms with Zn_3, generated a small increment in the activation free energy of the phosphoserine hydrolysis reaction (Table 2). As this mechanistic step is rate-determining for aryl phosphate substrates,[14,16−18] these observations would explain the lower activity of APs when Zn^{2+} instead of Mg^{2+} is present at the M3 site.[7−10]

A Mg^{2+}-bound hydroxide ion has been suggested to act as a general base to deprotonate the Ser92 nucleophile.[6,11] Nevertheless, other studies are not consistent with this general base catalysis model, proposing that the Mg^{2+} ion indirectly stabilizes the transferred phosphoryl group via a coordinated water ligand.[12] According to the present calculations, in the Michaelis noncovalent complex for both M3-Mg and M3-Zn proteins, the hydroxyl group of nucleophilic Ser92 was characterized as ionized, due to proton transfer to the initial hydroxide anion coordinated to the M3 metal cation. Hence, the activation of APs when magnesium is at the M3 site would not be explained by the general base catalysis model. However, a water molecule coordinated to Mg^{2+} (the one initially included as a hydroxide anion) was hydrogen-bonded to an oxygen atom of the phosphate group during the whole enzymatic mechanism. This hydrogen bond was also observed for the M3-Zn protein when Zn_3 was octahedrally coordinated, but it disappeared when the active site reorganized to adopt Zn_3-pentacoordination (from Step 2 in Scheme 2). This stabilizing interaction is equivalent to the one proposed by Zalatan et al.,[12] even though direct stabilization of the phosphoseryl group by Zn_3 appears to be the primary reason of the lower activity observed for M3-Zn APs.

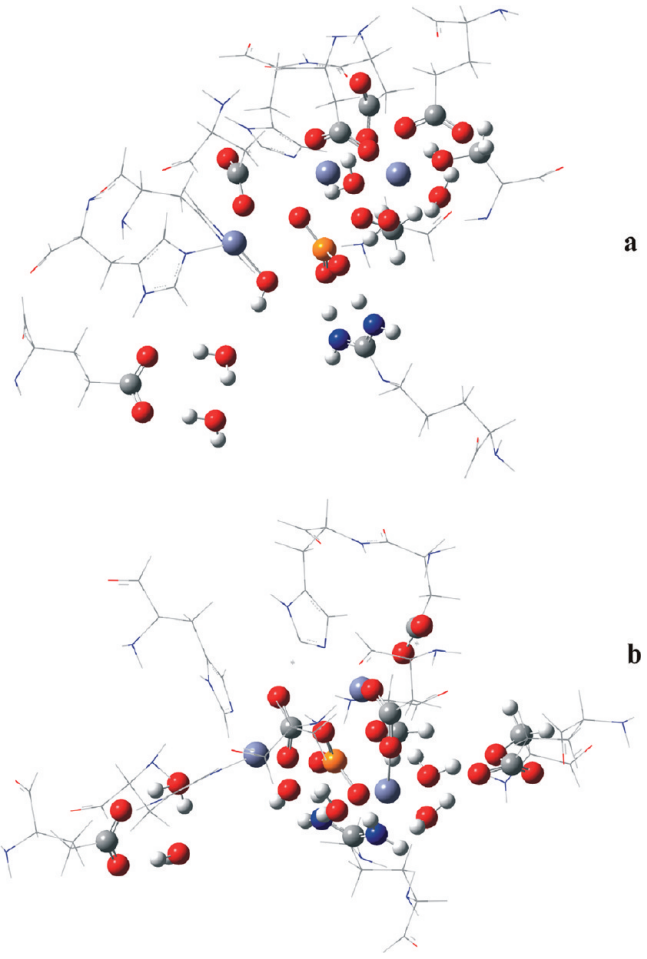

Figure 4. Transition states for hydrolysis of the covalent phosphoserine intermediate for the Zn_3 enzyme. (a) Highest energy TS (octahedral hexacoordination for Zn_3). (b) Lowest energy TS (square pyramidal pentacoordination for Zn_3).

In summary, the results from this computational study indicate that activation of APs by magnesium at the M3 site is caused by the preference of Mg for octahedral coordination, which structurally stabilizes the active site in a catalytically most active conformation. In contrast, reorganization of the active site due to a pentacoordinated zinc ion at M3 further stabilizes the covalent

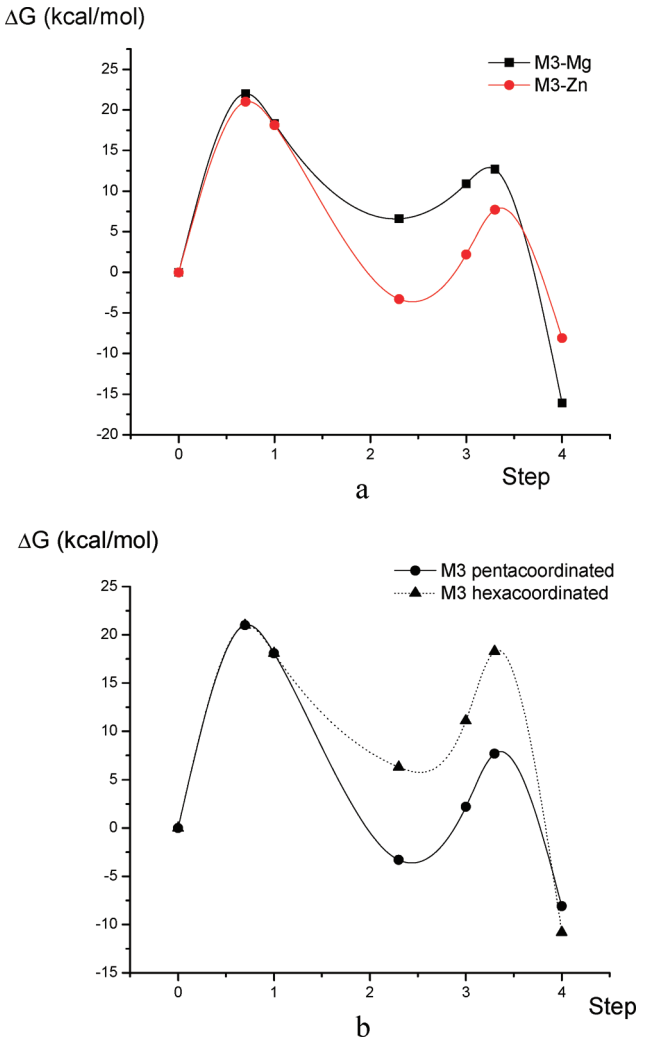

Figure 5. Free energy profiles for the mechanism in Scheme 2. (a) Comparison between the wild-type enzyme (M3-Mg) and the M3-Zn protein. (b) Comparison between square pyramidal pentacoordination and octahedral hexacoordination for Zn_3.

phosphoserine intermediate and hinders its hydrolysis, which is the rate-determining step for aryl phosphate substrates.

SUMMARY AND CONCLUSIONS

Computational results in the present study showed minimal changes in the atomic positions of the residues included in the PLAP model throughout the catalytic mechanism. This fact denotes that the active site organization of this enzyme is optimal to assist the hydrolysis of phosphate monoesters. The calculated activation and reaction energy and free energy values indicated that the nucleophilic attack of the Ser92 alkoxide on the phosphorus atom of the substrate would be the rate-limiting step of the catalytic hydrolysis of alkyl phosphate monoesters by PLAP. This observation is in accordance with previous experimental results.[59] Furthermore, the present calculations agree with the catalytic proficiencies assessed for APs.[63]

The reactivities of the wild-type M3-Mg enzyme and the M3-Zn protein were compared. The computed energies and free energies for the first chemical step of the catalytic mechanism were equivalent for both proteins differing in the M3 metal. However, the main difference between them was a change in the coordination number of M3 for the M3-Zn enzyme, observed after formation of the phosphoserine intermediate. Thus, the coordination sphere of Zn_3 changed from an octahedral (hexacoordinated) geometry to square pyramidal pentacoordination. This modification in the active site structure lowered the energy profile for the second chemical step of the catalytic mechanism (hydrolysis of the covalent phosphoserine intermediate). As a consequence, a greater stabilization of the phosphoseryl moiety resulted in a small increment in the activation free energy of the phosphoserine hydrolysis reaction. As this mechanistic step is rate-determining for aryl phosphate substrates,[14,16−18] these remarks are in line with the lower activity of APs when Zn^{2+} instead of Mg^{2+} is present at the M3 site.[7−10]

Therefore, these computational results suggest that activation of APs by magnesium at the M3 site is caused by the preference of Mg for octahedral coordination, which structurally stabilizes the active site in a catalytically most active conformation. On the other hand, a pentacoordinated zinc ion at M3 further stabilizes the covalent phosphoserine intermediate and thus hinders the hydrolysis step, as it has been observed with aryl phosphate substrates.[7−10]

The different computational methods employed in this work (quantum-mechanical calculations, molecular docking techniques, and MD simulations) complemented each other and afforded matching results. Reproduction of experimental observations is a useful way of testing the applicability and accuracy of theoretical methods and of assuring their predictive capability. In this way, the concordance between the present theoretical results and experimentally determined mechanistic features could be considered a good indication of the reliability of the calculations reported in this work. Related computational studies involving an aryl phosphate monoester as a substrate are currently in progress.

AUTHOR INFORMATION

Corresponding Author

*Phone: +54-351-434-4972. Fax: +54-351-434-4971. E-mail: gborosky@fcq.unc.edu.ar.

ACKNOWLEDGMENT

Financial support from Consejo Nacional de Investigaciones Científicas y Técnicas (CONICET) and the Secretaría de Ciencia y Tecnología de la Universidad Nacional de Córdoba (Secyt-UNC) is gratefully acknowledged.

REFERENCES

(1) McComb, R. B.; Bowers, G. N., Jr.; Posen, S. Measurement of alkaline phosphatase activity. In *Alkaline Phosphatases*; Plenum Press: New York, 1979; pp 986−989.

(2) Schwartz, J. H.; Lipmann, F. Phosphate incorporation into alkaline phosphatase of *E. coli*. *Proc. Natl. Acad. Sci. U.S.A.* **1961**, *47*, 1996–2005.

(3) Millán, J. L. *Mammalian alkaline phosphatases: From biology to applications in medicine and biotechnology*; Wiley-VCH Verlag GmbH & Co.: Weinheim, Germany, 2006; pp 1−322.

(4) Kim, E. E.; Wyckoff, H. W. Structure of alkaline phosphatases. *Clin. Chim. Acta* **1990**, *186*, 175–178.

(5) Murphy, J. E.; Tibbitts, T. T.; Kantrowitz, E. R. Mutations at positions 153 and 328 in *Escherichia coli* alkaline phosphatase provide insight towards the structure and function of mammalian and yeast alkaline phosphatases. *J. Mol. Biol.* **1995**, *253*, 604–617.

(6) Kim, E. E.; Wyckoff, H. W. Reaction mechanism of alkaline phosphatase based on crystal structures: Two-metal ion catalysis. *J. Mol. Biol.* **1991**, *218*, 449–464.

(7) Anderson, R. A.; Bosron, W. F.; Kennedy, F. S.; Vallee, B. L. Role of magnesium in *Escherichia coli* alkaline phosphatase. *Proc. Natl. Acad. Sci. U.S.A.* **1975**, *72*, 2989–2993.

(8) Xu, X.; Kantrowitz, E. R. Binding of magnesium in a mutant *Escherichia coli* alkaline phosphatase changes the rate-determining step in the reaction mechanism. *Biochemistry* **1993**, *32*, 10683–10691.

(9) Tibbitts, T. T.; Murphy, J. E.; Kantrowitz, E. R. Kinetic and structural consequences of replacing the aspartate bridge by asparagine in the catalytic metal triad of *Escherichia coli* alkaline phosphatase. *J. Mol. Biol.* **1996**, *257*, 700–715.

(10) Hung, H.-C.; Chang, G.-G. Differentiation of the slow-binding mechanism for magnesium ion activation and zinc ion inhibition of human placental alkaline phosphatase. *Protein Sci.* **2001**, *10*, 34–45.

(11) Stec, B.; Holtz, K. M.; Kantrowitz, E. R. A revised mechanism for the alkaline phosphatase reaction involving three metal ions. *J. Mol. Biol.* **2000**, *299*, 1303–1311.

(12) Zalatan, J. G.; Fenn, T. D.; Herschlag, D. Comparative enzymology in the alkaline phosphatase superfamily to determine the catalytic role of an active-site metal ion. *J. Mol. Biol.* **2008**, *384*, 1174–1189.

(13) Holtz, K. M.; Kantrowitz, E. R. The mechanism of the alkaline phosphatase reaction: insights from NMR, crystallography and site-specific mutagenesis. *FEBS Lett.* **1999**, *462*, 7–11.

(14) Reid, T. W.; Wilson, I. B. *Escherichia coli* alkaline phosphatase. In *The Enzymes*; Boyer, P. D., Ed.; Academic Press: New York, 1971; Vol. 4, pp 373−415.

(15) Coleman, J. E. Structure and mechanism of alkaline phosphatase. *Annu. Rev. Biophys. Biomol. Struct.* **1992**, *21*, 441–483.

(16) Bloch, W.; Gorby, M. S. Catalytic mechanism of *Escherichia coli* alkaline phosphatase: Resolution of three variants of the acyl-enzyme mechanism. *Biochemistry* **1980**, *19*, 5008–5018.

(17) Gettins, P.; Coleman, J. E. 31P nuclear magnetic resonance of phosphoenzyme intermediates of alkaline phosphatase. *J. Biol. Chem.* **1983**, *258*, 408–416.

(18) Hull, W. E.; Halford, S. E.; Gutfreund, H.; Sykes, B. D. Phosphorus-31 nuclear magnetic resonance study of alkaline phosphatase: The role of inorganic phosphate in limiting the enzyme turnover rate at alkaline pH. *Biochemistry* **1976**, *15*, 1547–1561.

(19) Hummer, C.; Millán, J. L. Gly429 is the major determinant of uncompetitive inhibition of human germ cell alkaline phosphatase by *L*-leucine. *Biochem. J.* **1991**, *274*, 91–95.

(20) LeDu, M. H.; Stigbrand, T.; Taussig, M. J.; Ménez, A.; Stura, E. A. Crystal structure of alkaline phosphatase from human placenta at 1.8 Å resolution. *J. Biol. Chem.* **2001**, *276*, 9158–9165.

(21) Makiya, R.; Stigbrand, T. Placental alkaline phosphatase has a binding site for the human immunoglobulin-G Fc portion. *Eur. J. Biochem.* **1992**, *205*, 341–345.

(22) Makiya, R.; Stigbrand, T. Placental alkaline phosphatase is related to human IgG internalization in HEp2 cells. *Biochem. Biophys. Res. Commun.* **1992**, *182*, 624–630.

(23) Stefaner, I.; Stefanescu, A.; Hunziker, W.; Fuchs, R. Expression of placental alkaline phosphatase does not correlate with IgG binding, internalization and transcytosis. *Biochem. J.* **1997**, *327*, 585–592.

(24) She, Q.-B.; Mukherjee, J. J.; Huang, J.; Crilly, K. S.; Kiss, Z. Growth factor-like effects of placental alkaline phosphatase in human fetus and mouse embryo fibroblasts. *FEBS Lett.* **2000**, *469*, 163–167.

(25) She, Q.-B.; Mukherjee, J. J.; Chung, T.; Kiss, Z. Placental alkaline phosphatase, insulin, and adenine nucleotides or adenosine synergistically promote long-term survival of serum-starved mouse embryo and human fetus fibroblasts. *Cell. Signal* **2000**, *12*, 659–665.

(26) Lin, S.; Sartori, M. J.; Mezzano, L.; de Fabro, S. P. Placental alkaline phosphatase (PLAP) enzyme activity and binding to IgG in Chagas' disease. *Placenta* **2005**, *26*, 789–795and references therein.

(27) Fishman, W. H.; Inglis, N. R.; Stolbach, L. L.; Krant, M. J. A serum alkaline phosphatase isoenzyme of human neoplastic cell origin. *Cancer Res.* **1968**, *36*, 935–938.

(28) Dempo, K.; Elliot, K. A. C.; Desmond, W.; Fishman, W. H. Demonstration of gamma-glutamyl transferase, alkaline phosphatase, CEA and HCG in human lung cancer. *Oncodev. Biol. Med.* **1981**, *2*, 21–37.

(29) Nouwen, E. J.; Pollet, D. E.; Schelstraete, J. B.; Eerdekens, M. W.; Hänsch, C.; Van de Voorde, A.; De Broe, M. E. Human placental alkaline phosphatase in benign and malignant ovarian neoplasia. *Cancer Res.* **1985**, *45*, 892–902.

(30) Nouwen, E. J.; Pollet, D. E.; Eerdekens, M. W.; Hendrix, P. G.; Briers, T. W.; De Broe, M. E. Immunohistochemical localization of placental alkaline phosphatase, carcinoembryonic antigen, and cancer antigen 125 in normal and neoplastic human lung. *Cancer Res.* **1986**, *46*, 866–876.

(31) Wick, M. R.; Swanson, P. E.; Manivel, J. C. Placental-like alkaline phosphatase reactivity in human tumors: An immunohistochemical study of 520 cases. *Hum. Pathol.* **1987**, *18*, 946–954.

(32) Guex, N.; Peitsch, M. C. SWISS-MODEL and the Swiss-Pdb Viewer: An environment for comparative protein modeling. *Electrophoresis* **1997**, *18*, 2714–2723.

(33) Jorgensen, W. L.; Chandrasekhar, J.; Madura, J. D.; Impey, R. W.; Klein, M. L. Comparison of simple potential functions for simulating liquid water. *J. Chem. Phys.* **1983**, *79*, 926–935.

(34) Hess, B.; Kutzner, C.; van der Spoel, D.; Lindahl, E. GROMACS 4: Algorithms for highly efficient, load-balanced, and scalable molecular simulation. *J. Chem. Theory Comput.* **2008**, *4*, 435–447.

(35) Hornak, V.; Abel, R.; Okur, A.; Strockbine, B.; Roitberg, A.; Simmerling, C. Comparison of multiple Amber force fields and development of improved protein backbone parameters. *Proteins* **2006**, *65*, 712–725.

(36) Wang, J.; Wang, W.; Kollman, P. A.; Case, D. A. Automatic atom type and bond type perception in molecular mechanical calculations. *J. Mol. Graphics Modell.* **2006**, *25*, 247–260.

(37) Wang, J.; Wolf, R. M.; Caldwell, J. W.; Kollman, P. A.; Case, D. A. Development and testing of a general AMBER force field. *J. Comput. Chem.* **2004**, *25*, 1157–1174.

(38) Darden, T.; York, D.; Pedersen, L. Particle mesh Ewald: An N-log(N) method for Ewald sums in large systems. *J. Chem. Phys.* **1993**, *98*, 10089–10092.

(39) Essmann, U.; Perera, L.; Berkowitz, M. L.; Darden, T.; Lee, H.; Pedersen, L. G. A smooth particle mesh ewald potential. *J. Chem. Phys.* **1995**, *103*, 8577–8592.

(40) Berendsen, H. J. C.; Postma, J. P. M.; DiNola, A.; Haak, J. R. Molecular dynamics with coupling to an external bath. *J. Chem. Phys.* **1984**, *81*, 3684–3690.

(41) Bussi, G.; Donadio, D.; Parrinello, M. Canonical sampling through velocity rescaling. *J. Chem. Phys.* **2007**, *126*, 014101–7.

(42) Hess, B.; Bekker, H.; Berendsen, H. J. C.; Fraaije, J. G. E. M. LINCS: A linear constraint solver for molecular simulations. *J. Comput. Chem.* **1997**, *18*, 1463–1472.

(43) Humphrey, W.; Dalke, A.; Schulten, K. VMD: visual molecular dynamics. *J. Mol. Graphics* **1996**, *14*, 33–38.

(44) Morris, G. M.; Huey, R.; Lindstrom, W.; Sanner, M. F.; Belew, R. K.; Goodsell, D. S.; Olson, A. J. AutoDock4 and AutoDockTools4: Automated docking with selective receptor flexibility. *J. Comput. Chem.* **2009**, *30*, 2785–2791.

(45) Frisch, M. J.; Trucks, G. W.; Schlegel, H. B.; Scuseria, G. E.; Robb, M. A.; Cheeseman, J. R.; Montgomery, J. A., Jr.; Vreven, T.; Kudin, K. N.; Burant, J. C.; Millam, J. M.; Iyengar, S. S.; Tomasi, J.; Barone, V.; Mennucci, B.; Cossi, M.; Scalmani, G.; Rega, N.; Petersson, G. A.; Nakatsuji, H.; Hada, M.; Ehara, M.; Toyota, K.; Fukuda, R.; Hasegawa, J.; Ishida, M.; Nakajima, T.; Honda, Y.; Kitao, O.; Nakai, H.; Klene, M.; Li, X.; Knox, J. E.; Hratchian, H. P.; Cross, J. B.; Bakken, V.; Adamo, C.; Jaramillo, J.; Gomperts, R.; Stratmann, R. E.; Yazyev, O.; Austin, A. J.; Cammi, R.; Pomelli, C.; Ochterski, J. W.; Ayala, P. Y.; Morokuma, K.; Voth, G. A.; Salvador, P.; Dannenberg, J. J.; Zakrzewski, V. G.; Dapprich, S.; Daniels, A. D.; Strain, M. C.; Farkas, O.; Malick, D. K.; Rabuck, A. D.; Raghavachari, K.; Foresman, J. B.; Ortiz, J. V.; Cui, Q.; Baboul, A. G.; Clifford, S.; Cioslowski, J.; Stefanov, B. B.; Liu, G.;

Liashenko, A.; Piskorz, P.; Komaromi, I.; Martin, R. L.; Fox, D. J.; Keith, T.; Al-Laham, M. A.; Peng, C. Y.; Nanayakkara, A.; Challacombe, M.; Gill, P. M. W.; Johnson, B.; Chen, W.; Wong, M. W.; Gonzalez, C.; Pople, J. A. Gaussian 03, Revision B.05; Gaussian, Inc.: Wallingford, CT, 2003.

(46) Stewart, J. J. P. Optimization of parameters for semiempirical methods. I. Method. *J. Comput. Chem.* **1989**, *10*, 209–220.

(47) Dapprich, S.; Komáromi, I.; Byun, K. S.; Morokuma, K.; Frisch, M. J. A new ONIOM implementation in Gaussian98. Part I. The calculation of energies, gradients, vibrational frequencies and electric field derivatives. *J. Mol. Struct. (Theochem)* **1999**, *461−462*, 1–21.

(48) Becke, A. D. Density-functional thermochemistry. III. The role of exact exchange. *J. Chem. Phys.* **1993**, *98*, 5648–5652.

(49) Lee, C.; Yang, W.; Parr, R. G. Development of the Colle-Salvetti correlation-energy formula into a functional of the electron density. *Phys. Rev. B* **1988**, *37*, 785–789.

(50) Miehlich, B.; Savin, A.; Stoll, H.; Preuss, H. Results obtained with the correlation energy density functionals of Becke and Lee, Yang and Parr. *Chem. Phys. Lett.* **1989**, *157*, 200–206.

(51) Cancès, M. T.; Mennucci, V.; Tomasi, J. A new integral equation formalism for the polarizable continuum model: Theoretical background and applications to isotropic and anisotropic dielectrics. *J. Chem. Phys.* **1997**, *107*, 3032–3041.

(52) Mennucci, B.; Tomasi, J. Continuum solvation models: A new approach to the problem of solute's charge distribution and cavity boundaries. *J. Chem. Phys.* **1997**, *106*, 5151–5158.

(53) Mennucci, B.; Cancès, E.; Tomasi, J. Evaluation of solvent effects in isotropic and anisotropic dielectrics and in ionic solutions with a unified integral equation method: Theoretical bases, computational implementation, and numerical applications. *J. Phys. Chem. B* **1997**, *101*, 10506–10517.

(54) Tomasi, J.; Mennucci, B.; Cancès, E. The IEF version of the PCM solvation method: An overview of a new method addressed to study molecular solutes at the QM ab initio level. *J. Mol. Struct. (Theochem)* **1999**, *464*, 211–226.

(55) Siegbahn, P. E. M.; Himo, F. The quantum chemical cluster apprach for modeling enzyme reactions. *WIREs Comp. Mol. Sci.* **2011**, *1*, 323–336and references therein.

(56) Siegbahn, P. E. M.; Himo, F. Recent developments of the quantum chemical cluster apprach for modeling enzyme reactions. *J. Biol. Inorg. Chem.* **2009**, *14*, 643–451and references therein.

(57) Sekharan, S.; Morokuma, K. QM/MM study of the structure, energy storage, and origin of the bathochromic shift in vertebrate and invertebrate bathorhodopsins. *J. Am. Chem. Soc.* **2011**, *133*, 4734–4737.

(58) Llinas, P.; Stura, E. A.; Ménez, A.; Kiss, Z.; Stigbrand, T.; Millán, J. L. Le Du, M. H. Structural studies of human placental alkaline phosphatase in complex with functional ligands. *J. Mol. Biol.* **2005**, *350*, 441–451.

(59) ÓBrien, P. J.; Herschlag, D. Alkaline phosphatase revisited: Hydrolysis of alkyl phosphates. *Biochemistry* **2002**, *41*, 3207–3225.

(60) Holtz, K. M.; Stec, B.; Kantrowitz, E. R. A model of the transition state in the alkaline phosphatase reaction. *J. Biol. Chem.* **1999**, *274*, 8351–8354.

(61) The classical transition-state theory expresses the rate constant for a reaction as $k = (k_BT/h)\ \exp(-\Delta G/RT)$, in which k_B is the Boltzmann constant, R is the gas constant, T is the absolute temperature, h is the Planck constant, and ΔG is the free energy of activation.

(62) Lad, C.; Williams, N. H.; Wolfenden, R. The rate of hydrolysis of phosphomonoester dianions and the exceptional catalytic proficiencies of protein and inositol phosphatases. *Proc. Natl. Acad. Sci. U.S.A.* **2003**, *100*, 5607–5610.

(63) ÓBrien, P. J.; Herschlag, D. Functional interrelationships in the alkaline phosphatase superfamily: Phosphodiesterase activity of *Escherichia coli* alkaline phosphate. *Biochemistry* **2001**, *40*, 5691–5699.

(64) Roe, R. R.; Pang, Y.-P. Zincś exclusive tetrahedral coordination governed by its electronic structure. *J. Mol. Model.* **1999**, *5*, 134–140.